Journal of Manufacturing Processes 109 (2024) 100–114

Contents lists available at ScienceDirect

Journal of Manufacturing Processes

journal homepage: www.elsevier.com/locate/manpro

Full length article

Multilevel variable control for impulse-discharge thermochemical truing of diamond cutting edges in precision grinding

Quanpeng He [a,b], Jin Xie [b,*], Jiaxin Chen [b], Hao Yang [b], Jiajun Huang [b], Hui Deng [a,*]

[a] Department of Mechanical and Energy Engineering, Southern University of Science and Technology, Shenzhen, Guangdong 518055, China
[b] Department of Mechanical and Automotive Engineering, South China University of Technology, Guangzhou, Guangdong 510000, China

ARTICLE INFO

Keywords:
Diamond grinding
Thermochemical truing
Impulse-discharge signal
Experiential knowledge
Fuzzy control

ABSTRACT

Precision grinding depends on the diamond cutting edges with good protrusion uniformity that are acquired by impulse-discharge thermochemical truing. However, the impulse-discharge thermal is unstable due to the uncertain discharge gap derived from irregularly changed grain top heights, leading to random diamond thermochemical removal. Under the uncertainty, a multilevel fuzzy-based control of kinematic and electrical variables is proposed to stabilize the impulse-discharge power during truing. The objective is to realize the cooperation of impulse-discharge, thermochemical and mechanical processes for diamond truing effect trace. First, the impulse-discharge signal was collected to acquire the transfer functions of impulse-discharge power. Then, an on-site experiment with small sample was processed to determine the discharge voltage sensitivities of kinematic and electrical variations. In order to improve the control performance, the control process with fuzzy logic was modeled to tune the output ratios of kinematic and electrical variations by particle swarm algorithm. Finally, the designed controller was experimentally applied to the impulse-discharge thermochemical truing, followed with dry plunge grinding of hardened steel. It is shown that the kinematic and electrical variables for the uncertainty compensation are linearly related to the spark-discharge voltage. Accordingly, the fuzzy-based control may be applied to the multilevel variable adjustment. The controller with tuned output ratios reaches small steady-state error, few trigger times and no overshoot to regulate the impulse-discharge power within 5 % error in actual truing. By integrating physical behavior and experiential knowledge rather than big data driving, the controllable impulse-discharge power for required diamond cutting edges advances the stable smooth surface grinding.

1. Introduction

Prior information is significant to advance the intelligent control of manufacturing system for the required product performance [1]. Moreover, smart manufacturing technologies depend on big data driving to adapt the random interactions between machine tool and workpiece, leading to a long-term accumulation [2]. In order to improve the traditional injection molding process, an intelligent knowledge-based system was developed to optimize the production manufacturing strategy for industrial productivity [3]. Based on the prior information of electrical discharge machining (EDM) process and machine tool, an experienced EDM specialist was utilized to perform the knowledge-based design of electrodes [4]. In efficient robotic manufacturing systems, a knowledge-based program-generation was proposed to support the rule standardization related to manufacturing programs [5]. However, these researches have not revealed the on-site status information of manufacturing process.

In order to machine the difficult-to-cut quartz, a knowledge logic chain of target surface quality, tool kinematic variables and grain protrusion information was introduced in feed-back control to improve the process effectiveness [6]. A multi-sensor monitoring was proposed to perform the wear assessment by modeling the relationships between ground surface roughness and measured process data such as grinding force components and acoustic emission signals [7]. Based on the coefficient fitting of Preston polishing theory, the knowledge logic extension of thermal and mechanical loads was considered to predict the workpiece damage and tool wear during grinding of pcBN [8]. The knowledge-based interaction of temperature parameters, radiation waveband and background radiation was introduced by Huang et al. [9] to predict the material-surface emissivity for dynamic temperature determination of belt grinding. However, the knowledge-based approaches have not been applied to online feed-back control of process

* Corresponding authors.
E-mail addresses: jinxie@scut.edu.cn (J. Xie), dengh@sustech.edu.cn (H. Deng).

https://doi.org/10.1016/j.jmapro.2023.11.038
Received 17 August 2023; Received in revised form 30 October 2023; Accepted 28 November 2023
Available online 14 December 2023

precision.

The precision manufacturing depends on various physical knowledge which may not be defined easily. Accordingly, some advanced algorithms are often applied to the manufacturing process control without describing complex physical behavior. For example, Tang et al. [10] modeled the mechanical vibration and acoustic signals for high-quality mineral grinding with a multi-layer selective ensemble algorithm. An online model identification with Levenberg-Marquardt algorithm was improved by Lee [11] to predict the ground surface roughness. Lee et al. [12] also utilized an artificial neural network to quantify the wheel dressing variables in precision grinding. By integrating active incremental fine-tuning, optimized SegNet and conditional random field, Ren et al. [13] monitored the tool wear to improve ground surface quality. However, big sample data is essential to be acquired for the feedback control in-process. Although Dai et al. [14] developed an adaptive proportional integral derivative (PID) controller with back-stepping method to stabilize the grinding force with small experiential data, the quick response produced unavoidable oscillation and more instability to grinding process.

Moreover, the fuzzy algorithm was first developed by Zadeh [15,16] to model the control process by associating linguistic variables derived from experiential knowledge rather than big sample data. In contrast to the PID approach, the fuzzy one is more suitable to integrate the multi-input/output signals of manufacturing system with less predefined controller parameters [17]. Based on the fuzzy control, the robot-assisted grinding of vertebral lamina with constant force was performed by Qi et al. [18] to obtain a high-quality finished surface in surgical operation. As the milling chatter was also influenced by process variables and system structure, Li et al. [19] designed a fuzzy controller of vibration displacements to achieve suitable actuator voltage for milling stability. To achieve high cutting accuracy, Lin et al. [20] employed the fuzzy control to compensate the deviated cutting trajectory by adjusting cutting feed rate. Until now, the controller designation has not concerned the precision manufacturing behavior.

To assure fuzzy control effect, Wang et al. [21] utilized the adaptive network to online tune the input/output ratios of fuzzy inference system for high-accuracy control of thin-walled milling, but the optimization depends on the size of training data set. For wellhead back pressure control, Liang et al. [22] employed the genetic algorithm to optimize fuzzy controller by a self-defined objective function rather than sample data driving, which achieved small rise time, adjustment time and no overshoot. Based on the behavior of bird foraging, a novel genetic algorithm of particle swarm optimization was developed by Kennedy et al. [23] to resolve the constraint optimization problem of multiple factors with fast convergence. By adding a mutant vector of particle search, the control parameters were efficiently tuned in fuel-cell temperature system to achieve high tracing accuracy [24]. For the high-value industrial requirement, integrating the manufacturing behavior into fuzzy control is necessary to assure the online accuracy compensation.

In difficult-to-cut metal grinding especially of ferrous materials, the irregular diamond cutting edges are easily graphitized by mechanical friction at low temperature [25], leading to the unstable precision process. Generally, the CBN grinding with good chemo-resistance replaces the diamond grinding to machine the ferrous materials for sub-micron surface roughness [26], but the coolants are required to lubricate the cutting interface. Based on the diamond thermal conductivity along with transmission balance on cutting interface, the impulse-discharge thermochemical truing was performed to truncate the diamond grain tops for cutting edge uniformity [27,28], which might achieve dry ground surface of hardened steel with 100-nm-*Ra* and less. It is also reported that the grain top area was positively correlated to the ground surface roughness. However, the fluctuating impulse-discharge power has not yet been controlled in the truing process to precisely trace the grain top area in reference to diamond thermochemical removal, leading to random improvement of ground surface quality. Although Brinksmeier et al. [29] and Wu et al. [30] also developed the on-machine removal of diamond grain tops by utilizing mechanical and laser-assisted truing, it is difficult to collect the process information for precision control.

In this study, a multilevel control of kinematic and electrical variables is proposed with fuzzy logic to stabilize the impulse-discharge power in thermochemical truing. The closed-loop control process is driven by integrating physical behavior and experiential knowledge rather than big sample data. Accordingly, the diamond truing effect trace is realized to acquire required diamond cutting edges for precision metal grinding. First, the impulse-discharge signal was characterized to acquire the transfer functions of impulse-discharge power; then, impulse-discharge voltage sensitivities of kinematic and electrical variations were determined by processing a small sample of on-site experimental data; next, the particle swarm algorithm was utilized in multilevel variable control model to tune the output ratios of kinematic and electrical variations intelligently for required control performance; finally, the designed controller was experimentally applied to the impulse-discharge thermochemical truing, followed with dry plunge grinding of hardened steel.

2. Multilevel variable control method on impulse-discharge thermochemical truing of diamond cutting edges

Precision grinding of difficult-to-cut metals depends on diamond cutting edges with good protrusion uniformity. Based on the graphitization temperature, an on-machine thermochemical truing of diamond cutting edges was performed by coupling the impulse-discharge thermal and mechanical friction thermal [28]. In the impulse-discharge thermochemical truing (see Fig. 1), the cutting chip height h_f is formed within grain top height h_g when the diamond grain cuts the electrode at the kinematic variables K of wheel speed N, feed rate v_f and cutting depth a_p, triggering an impulse-discharge through the electrical variables E of open circuit voltage E_i and limited current I_i in the discharge gap G_e. Herein, the impulse-discharge thermal is positively related to the discharge gap G_e. For the specific truing variables, the discharge gap G_e, however, reveals an uncertainty as the increasing truing time t_c. This phenomenon is mainly attributed to the random change of grain top height h_g from diamond thermochemical removal and wheel bond removal, then to the occasional chip accumulation or shedding grain. Consequently, the fluctuating impulse-discharge cannot guarantee the grain graphitization and result in random truing effect.

The fluctuating impulse-discharge, including the voltage and current signal, has been observed with increasing the truing time t_c in the previous research (see Fig. 1). For the impulse-discharge produced by DC power supply, the discharge voltage U_c could be quantified as the mean of voltage signal values $U_c^{(i)}$, that is $U_c = (U_c^{(1)} + U_c^{(2)} + \ldots + U_c^{(i)})/i$, and the discharge current I_c could be quantified as the mean of pulse peak values of current signal $I_c^{(i)}$, that is $I_c = (I_c^{(1)} + I_c^{(2)} + \ldots + I_c^{(i)})/i$. Herein, the pulses of current signal with low peak value and extremely short duration are taken as the disturbance from current sensor, which could be neglected. Based on the experiential knowledge, the thermochemical truing of diamond cutting edges has been quantified by grain top area s_g, and associated with the impulse-discharge power P by considering the thermal distribution between diamond grain, wheel bond and electrode. Accordingly, the impulse-discharge power P, calculated by $P = U_c \times I_c$, is determined as the key controlled object in this study. Further the corresponding linear correlations to truing variables of kinematic variables K and electrical variables E could be utilized to compensate the grain protrusion uncertainty for controllable P.

Fig. 1 also shows the designed multilevel variable control system framework of impulse-discharge thermochemical truing. For the required diamond cutting edges in precision grinding, a target impulse-discharge power P_{tar} is set by utilizing the developed physical behavior. The P is characterized from the traced impulse-discharge signal to obtain impulse-discharge power error e_p by comparing to the target value P_{tar}, and the e_p is further utilized to judge whether the controller should be implemented to adjust the truing variables (K, E) or not based on their

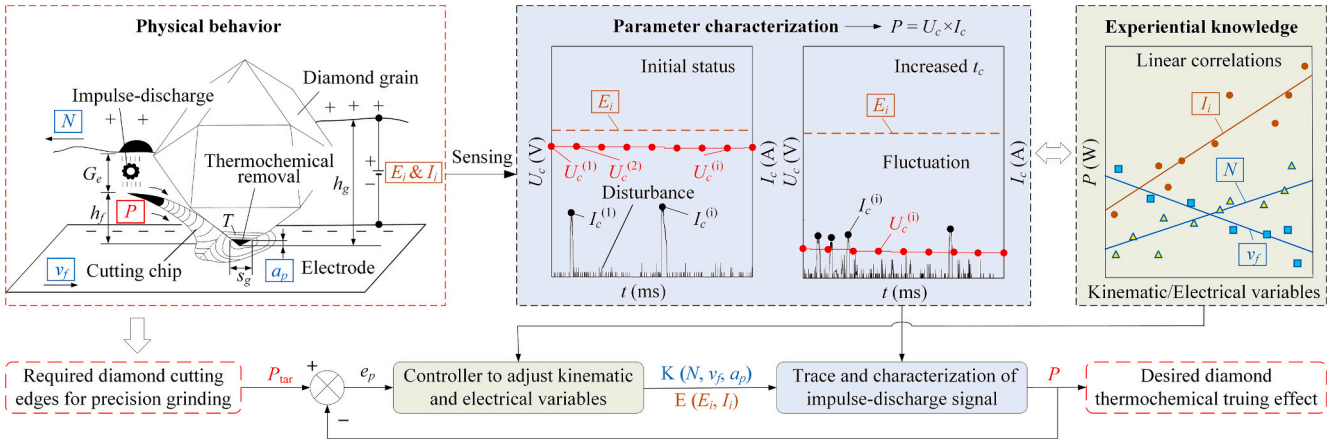

Fig. 1. Multilevel variable control system framework of impulse-discharge thermochemical truing based on physical behavior and experiential knowledge.

linear correlations. Accordingly, the impulse-discharge power P may be controlled to achieve desired diamond thermochemical truing effect.

The fuzzy method is proposed for impulse-discharge power control, and the three truing variables of wheel speed N, feed rate v_f and limited current I_i are advised in actual application. It is necessary to select an appropriate open circuit voltage E_i that suits the grain size. While the cutting depth a_p does not been adjusted by considering the system safety and the truing process stability. For multilevel variable control of impulse-discharge power, the physical models of grain cutting temperature rate T and grain top height h_g are utilized to determine system parameter initialization. Further, the standard triangular membership functions and their fuzzy rules of impulse-discharge power error e_p and truing variations (ΔK, ΔE) are designed by considering the experiential knowledge on impulse-discharge thermochemical truing. The corresponding scheme is described in Fig. 2 as follows:

1) The initial grain protrusion parameters including initial grain top height h_{g0} and area s_{g0}, etc. are given based on the wheel topography with grain size g_s. Further, the target impulse-discharge power P_{tar} is

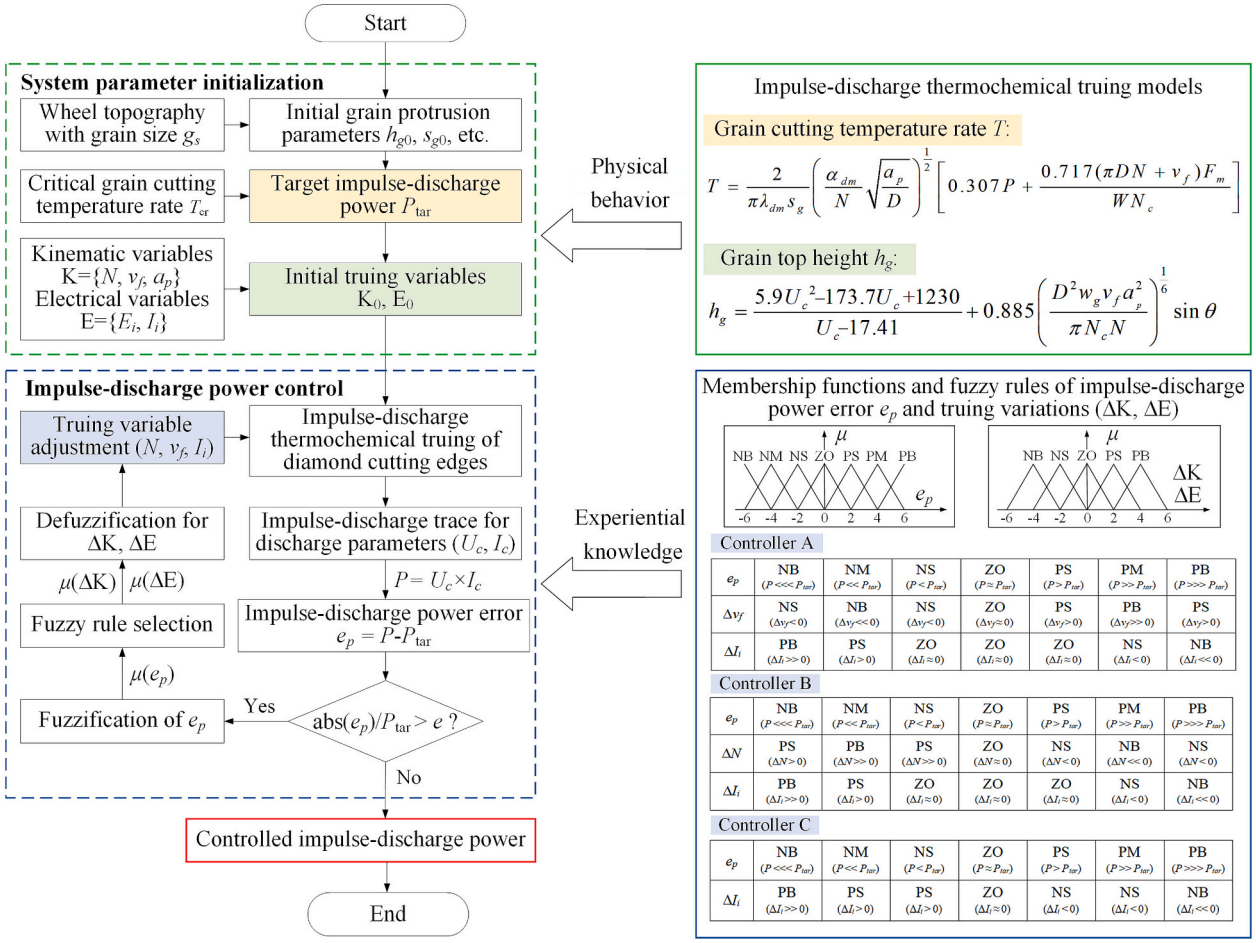

Fig. 2. Knowledge-based control scheme of impulse-discharge power P by kinematic variables K = {N, v_f, a_p} and electrical variables E = {E_i, I_i}.

calculated by utilizing a critical grain cutting temperature rate T_{cr} to set the initial truing variables (K_0, E_0).

2) The impulse-discharge thermochemical truing of diamond cutting edges is conducted with impulse-discharge trace, and the discharge parameters (U_c, I_c) are utilized to obtain the impulse-discharge power error e_p. When the impulse-discharge power relative error abs(e_p)/P_{tar} is beyond its threshold e, the designed controllers are triggered to adjust the truing variables $K = K_0 + \Delta K$ and $E = E_0 + \Delta E$.
3) For truing variables adjustment, the e_p is fuzzified to attain the corresponding membership $\mu(e_p)$, which is then utilized to determine the membership of truing variations $\mu(\Delta K)$ and $\mu(\Delta E)$ by selecting suitable fuzzy rule. Further, they are defuzzified to attain the new truing variables (K, E).

To analyze the diamond thermochemical removal mechanism, He et al. [28] has modeled the grain cutting temperature rate T with the impulse-discharge thermal from impulse-discharge power P and mechanical friction thermal from cutting force F_m. It is described as follows:

$$T = \frac{2}{\pi\lambda_{dm}s_g}\left(\frac{\alpha_{dm}}{N}\sqrt{\frac{a_p}{D}}\right)^{\frac{1}{2}}\left[0.307P + \frac{0.717(\pi DN + v_f)F_m}{WN_c}\right] \tag{1}$$

where D and W are wheel diameter and width. $\alpha_{dm} = 1110$ mm^2/s and $\lambda_{dm} = 2000$ W/m·K are the thermal diffusivity and thermal conductivity of diamond grain, respectively. Further, cutting force $F_m = 14$ N and active grain number for unit wheel width $N_c = 31$ were given in the impulse-discharge thermochemical truing of 350-μm-size diamond wheel.

For the thermal transmission balance on diamond cutting interface, the critical grain cutting temperature rate $T_{cr} = 51.6$ °C per wheel revolution of diamond graphitization was defined in reference to grain size [27]. Thus the target impulse-discharge power P_{tar} conforming to the required grain top area s_g is described as follows:

$$P_{tar} = 1.629\pi\lambda_{dm}T_{cr}s_g\left(\frac{N_{max}}{\alpha_{dm}}\sqrt{\frac{D}{a_{pmin}}}\right)^{\frac{1}{2}} - \frac{0.717(\pi DN_{max} + v_{fmin})F_m}{0.307WN_c} \tag{2}$$

where the maximum wheel speed $N_{max} = 3000$ rpm, minimum feed rate $v_{f\,min} = 10$ mm/min and cutting depth $a_{p\,min} = 1$ μm are utilized based on the adjustable ranges of $N \in [1800, 3000]$, $v_f \in [10, 150]$ and $a_p \in [1, 4]$. This is because the truing system should provide enough impulse-discharge power P for diamond thermochemical removal at each truing variable adjustment.

Besides, He et al. [27] modeled the grain top height h_g by associating cutting chip height h_f with spark-discharge gap G_e in constant-current mode ($U_c < E_i$). When the open circuit voltage $E_i = 25$ V and limited current $I_i = 0.1$ A are set, the h_g is described as follows:

$$h_g = G_e + h_f = f(U_c) + 0.885\left(\frac{D^2w_gv_fa_p^2}{\pi N_cN}\right)^{\frac{1}{6}}sin\theta \tag{3a}$$

$$f(U_c) \approx \frac{5.9U_c^2 - 173.7U_c + 1230}{U_c - 17.41}, \quad U_c \in [18, 25] \tag{3b}$$

where grain top width $w_g = 107$ μm and cutting chip angle $\theta = 34.4°$ were taken as constants in the impulse-discharge thermochemical truing of 350-μm-size diamond wheel.

Through the critical discharge voltage at target impulse-discharge power P_{tar}, the initial kinematic variables $K_0 = \{N_0, v_{f0}, a_{p0}\}$ conforming to the initial grain top height h_{g0} at the beginning of truing are described as follows:

$$\frac{2.08\pi N_c}{D^2w_g}\left[\frac{h_{g0} - f(U_{cmax})}{sin\theta}\right]^6 \le \frac{v_{f0}}{N_0}a_{p0}^2 \le \frac{2.08\pi N_c}{D^2w_g}\left[\frac{h_{g0} - f(U_{cmin})}{sin\theta}\right]^6 \tag{4}$$

where U_{cmax} and U_{cmin} are the maximum and minimum discharge voltage, respectively.

3. Multilevel variable control model of impulse-discharge power

3.1. Structure of multilevel variable control model

The multilevel variable control model including error calculation, fuzzy controller design, output ratio definition, truing variable adjustment and signal trace is developed as shown in Fig. 3. Three controllers are designed to calculate impulse-discharge power variation ΔP through transfer function. Considering that the small fluctuation of impulse-discharge power is generally observed in actual truing, and then large kinematic variations may induce mechanical vibration, thus the impulse-discharge power error e_p for each control is set not more than ± 10 W. Controller A is preferentially utilized to attain the feed rate variation Δv_f and limited current variation ΔI_i in reference to the e_p. When the accumulated Δv_f is beyond ± 70 mm/min, controller B is further utilized to attain the wheel speed variation ΔN and limited current variation ΔI_i. When the accumulated ΔN is also beyond ± 600 rpm, controller C is finally utilized to attain the limited current variation ΔI_i. The accumulated ΔI_i from the three controllers is not more than ± 0.08 A. Considering that the trigger judgment of multilevel variable control may conduct with a certain interval for actual application due to the limited system response time on microsecond impulse-discharge regulation, thus a trigger delay is set in the model. A time-varying signal module is also set to simulate disturbed impulse-discharge power P_0 related to the uncertain grain protrusion. Thus the simulative impulse-discharge power P is described as follows:

$$P = P_0 + \Delta P_{vf} + \Delta P_N + \Delta P_{Ii} \tag{5}$$

where ΔP_{vf}, ΔP_N and ΔP_{Ii} are impulse-discharge power variations related to feed rate, wheel speed and limited current, respectively.

Besides, the fuzzy rules of three controllers are designed by utilizing the correlation between discharge parameters (U_c, I_c) and truing variables (K, E). For instances, some fuzzy rules of controller A in Fig. 2 can be expressed as follows:

Rule 1: IF (e_p is NB) THEN (Δv_f is NS) AND (ΔI_i is PB).

Rule 2: IF (e_p is NM) THEN (Δv_f is NB) AND (ΔI_i is PS).

3.2. Transfer function of impulse-discharge power related to truing variables

In the impulse-discharge thermochemical truing system, the truing variables dominate the impulse-discharge formation, thus a discharge voltage sensitivity u is defined related to truing variations (ΔK, ΔE). The constant-voltage mode ($U_c = E_i$) is transformed into the constant-current mode ($U_c < E_i$) when the impulse-discharge happens at the sampling time $t = t_0$ (see Fig. 4a). Although the first discharge current I_c is triggered without any delay, there exists a response time to make the discharge voltage U_c decrease from the set open circuit voltage E_i to stable value. Herein, a small damped oscillation of U_c is also observed by magnifying the resolution of impulse-discharge trace. However, it is difficult to directly describe the dynamic characteristics of impulse-discharge due to system complexity. Accordingly, the difference δU_c between open circuit voltage E_i and discharge voltage U_c at a sampling time t is obtained to draw an underdamped step response curve as shown in Fig. 4b. When it begins at $t = t_0$, the controlled object of δU_c is described by a second order transfer function $G_u(s)$ as follows:

$$G_u(s) = u\frac{Y(s)}{R(s)} = \frac{u}{T_0^2s^2 + 2\xi T_0s + 1} = \frac{u\omega_n^2}{s^2 + 2\xi\omega_ns + \omega_n^2} \tag{6}$$

where T_0 is time constant of response system, ζ is damping ratio, $\omega_n = 1/T_0$ is undamped natural oscillation frequency. In this study, the wheel speed N, feed rate v_f and limited current I_i are adjusted to regulate impulse-discharge power, thus the discharge voltage sensitivity of u_N, u_{vf}

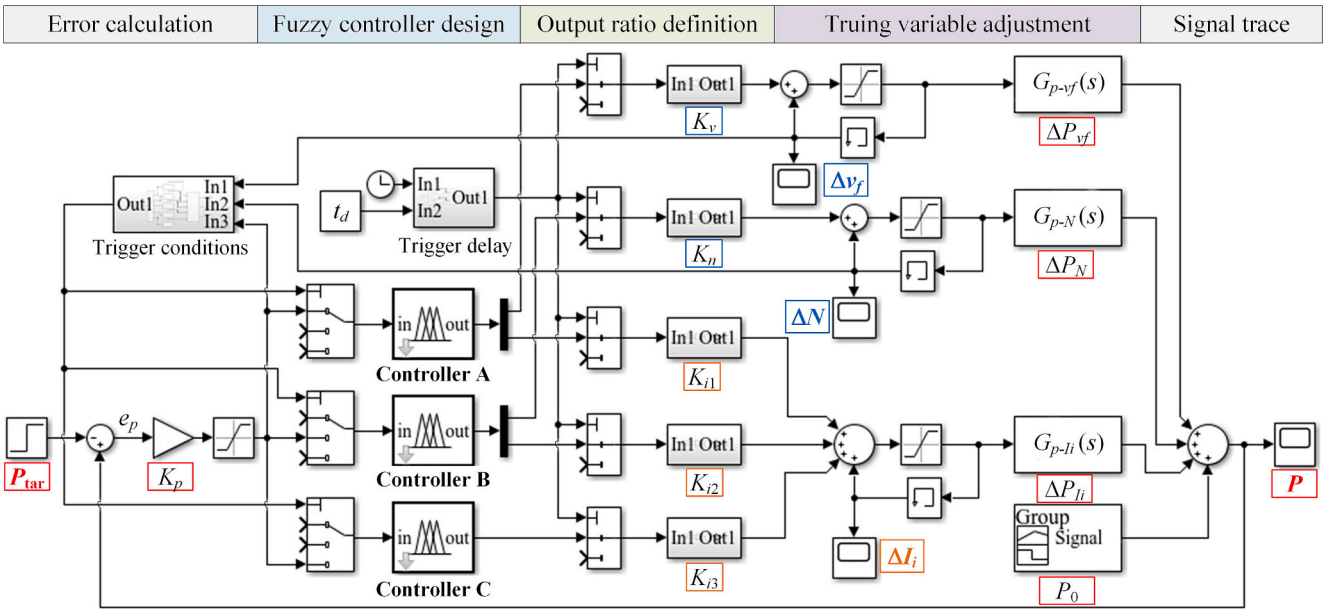

Fig. 3. Multilevel variable control model of impulse-discharge power P by utilizing the truing variables of feed rate v_f, wheel speed N and limited current I_i.

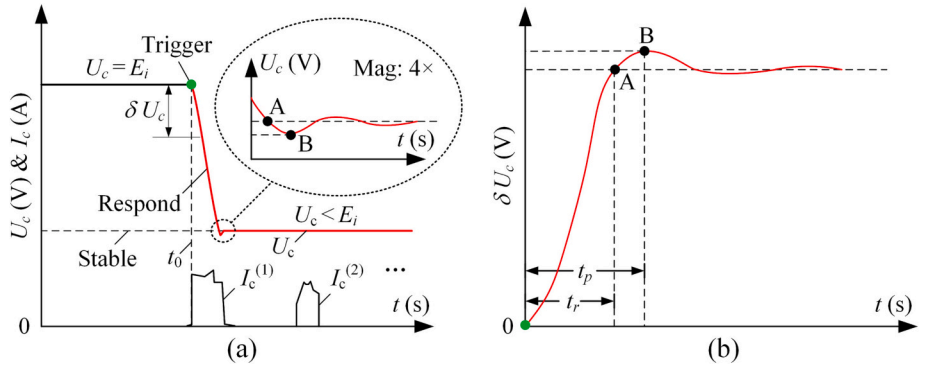

Fig. 4. Dynamic characteristics of impulse-discharge during truing. (a) Impulse-discharge waveform. (b) Underdamped step response of δU_c.

and u_{Ii} are given by experimental results.

It should be indicated that the system response time of each truing variable adjustment is almost the same. This is because the impulse-discharge happening in the gap mainly depends on the DC power supply. Although the wheel speed N and feed rate v_f may regulate the impulse-discharge by changing the discharge gap, the gap formation time is extremely short for each diamond grain cutting (<10 μs) which could be neglected in contrast to the millimeter response time of DC power supply. When the DC power supply, the grinder and the diamond wheel are determined for system control, the response time of truing variations (ΔK, ΔE) in the Eq. (6) may be taken as constant.

For impulse-discharge thermochemical truing of 350-μm-size diamond wheel, the suitable range of discharge voltage U_c = 19–23 V and current I_c = 2–4 A were determined by He et al. [28] to produce spark-discharge in the constant-current mode ($U_c < E_i$). To simplify calculation of multilevel variable control model, the I_c = 3 A is taken as a constant. The transfer function of impulse-discharge power $G_p(s)$ is described as follows:

$$G_p(s) = \frac{uI_c\omega_n^2}{s^2 + 2\xi\omega_n s + \omega_n^2} \tag{7}$$

Generally, the second order transfer function for unit step response is described as follows:

$$y(s) = \frac{1}{T_0^2 s^2 + 2\xi T_0 s + 1} \times \frac{1}{s} = \frac{1}{s} - \frac{s + \xi\omega_n}{(s + \xi\omega_n)^2 + \omega_d^2} - \frac{\xi\omega_n}{(s + \xi\omega_n)^2 + \omega_d^2} \tag{8}$$

where $\omega_d = \omega_n\sqrt{1-\xi^2}$ is damped oscillation angular frequency.

Through inverse Laplace transform, Eq. (8) is described as follows:

$$y(t) = 1 - \frac{1}{\sqrt{1-\xi^2}} e^{-\xi\omega_n t} sin\left(\sqrt{1-\xi^2}\,\omega_n t + arctan\frac{\sqrt{1-\xi^2}}{\xi}\right) \tag{9}$$

According to the rise time t_r in unit step response, let $y(t_r) = 1$. Thus the t_r is given as follows:

$$t_r = \frac{\pi - arctan\left(\frac{\sqrt{1-\xi^2}}{\xi}\right)}{\omega_n\sqrt{1-\xi^2}} \tag{10}$$

Further, according to the peak time t_p in unit step response, let $\frac{d_{y(t)}}{d_t}\Big|_{t=t_p} = 0$. Thus the t_p is given as follows:

$$t_p = \frac{\pi}{\omega_n\sqrt{1-\xi^2}} \tag{11}$$

In terms of Eqs. (10) and (11), the ξ and ω_n are given, respectively, as follows:

$$\xi = \frac{1}{\sqrt{tan^2\left(\pi - \frac{\pi t_p}{t_p}\right) + 1}} \tag{12}$$

$$\omega_n = \frac{\pi\sqrt{tan^2\left(\pi - \frac{\pi t_r}{t_p}\right) + 1}}{t_p tan^2\left(\pi - \frac{\pi t_r}{t_p}\right)} \tag{13}$$

Substituting Eqs. (12) and (13) into Eq. (7), the $G_p(s)$ is described as follows:

$$G_p(s) = \frac{uI_c\pi^2\left[tan^2\left(\pi - \frac{\pi t_r}{t_p}\right) + 1\right]}{{t_p}^2 tan^4\left(\pi - \frac{\pi t_r}{t_p}\right)s^2 + 2\pi t_p tan^2\left(\pi - \frac{\pi t_r}{t_p}\right)s + \pi^2 tan^2\left(\pi - \frac{\pi t_r}{t_p}\right) + \pi^2} \tag{14}$$

3.3. Intelligent tuning of output ratios by particle swarm algorithm

Based on the generally observed variation range of impulse-discharge power $P\in$ [35, 85] in the truing process, the impulse-discharge power error e_p can be divided into two symmetric intervals of $e_p\in$ [−25, −1] and $e_p\in$ [1, 25] at the target impulse-discharge power $P_{tar} = 60$ W. Due to the limited impulse-discharge power error e_p of ±10 W for each control, the corresponding input ratio K_p in Fig. 3 is set as 0.6, while the particle swarm algorithm [23] is employed to determine the five output ratios of feed rate variation K_v, wheel speed variation K_n and limited current variation $K_{i1,\,2,\,3}$ in the range of 0.1 to 5. It is necessary to make the absolute steady-state error e_s, trigger time t_p and overshoot O_p of impulse-discharge power under the multilevel variable control as small as possible. Herein, the e_s and the O_p should be close to zero to make the impulse-discharge power stabilize at the target value, while the t_p should be close to one to achieve an efficient control. Thus the objective function for each impulse-discharge power error is defined as follows:

$$f_{obj} = \eta_1\frac{e_s - e_{smin}}{e_{smax} - e_{smin}} + \eta_2\frac{t_p - t_{pmin}}{t_{pmax} - t_{pmin}} + \eta_3\frac{O_p - O_{pmin}}{O_{pmax} - O_{pmin}} \tag{15}$$

where f_{obj} is individual fitness value, $\eta_{1,\,2,\,3}$ are weights of steady-state error, trigger time and overshoot, respectively. Considering that the e_s associated with the trace precision of grain top area is taken as the most important factor during truing, followed by the t_p associated with the control efficiency. While the O_p associated with the control process stability is less important due to the slightly fluctuating impulse-discharge power derived from irregularly distributed diamond grains. Accordingly, the $\eta_1 = 50$ %, $\eta_2 = 30$ % and $\eta_3 = 20$ % are set in this study. Further, the available ranges of $e_s\in$ [0, 5], $t_p\in$ [1, 6] and $O_p\in$ [0, 5] are determined for the requirement of impulse-discharge power control. When $e_s > 5$ W or $t_p > 6$ or $O_p > 5$ W, the $f_{obj} = 1$.

In the case of impulse-discharge power errors $e_p\in$[−25, −1] and $e_p\in$[1, 25], their individual fitness values f_{obj} are same due to the symmetry of designed fuzzy rules. To simplify analysis process, the $e_p = 1, 2, \ldots, 25$ W are selected to determine the output ratios, which is when the disturbed impulse-discharge power $P_0 = 61, 62, \ldots, 85$ W. Accordingly, a total fitness value F_{obj} is given to evaluate the applicability of output ratios as follows:

$$F_{obj} = \eta_4\sum_{u=1}^{15} f_{obj}^{(u)} + \eta_5\sum_{u=1}^{10} f_{obj}^{(u+15)} \tag{16}$$

where $\eta_{4,\,5}$ are weights of individual fitness value for $e_p = 1$–15 W and $e_p = 16$–25 W, respectively. Considering that the nanoscale change of grain top height per wheel revolution in the thermochemical truing generally produces a small fluctuation of impulse-discharge power, while the chip accumulation or shedding grain does not happen frequently to produce a large fluctuation of impulse-discharge power. Accordingly, the $\eta_4 = 80$ %, $\eta_5 = 20$ % are also set in this study.

To describe the change of population particles in the particle swarm optimization algorithm, an evolutionary velocity v_p was determined by Juang et al. [31] as follows:

$$\begin{aligned} v_p^{(i,j)} &= v_p^{(i-1,j)} + c_1 rand_1\left(p_{best}{}^{(j)} - p^{(i,j)}\right) + c_2 rand_2\left(p_{gbest} - p^{(i,j)}\right) \\ &\quad i = \{1, 2, \ldots, n_{cmax} - 1\}, j = \{1, 2, \ldots, n_{pt}\} \end{aligned} \tag{17}$$

where p and p_{best} are current position and partial best position of single particle, p_{gbest} is global best position of all the particles, n_{cmax} is maximum iterations, n_{pt} is total particle number, $rand_{1,\,2}\in$[0, 1] are uniformly random numbers, respectively. In this study, the positive constants $c_{1,2} = 2$ and $v_p^{(0,\,j)} = 0$ are given for calculation.

Accordingly, the new population particles X are generated and theirs position p is calculated by utilizing the evolutionary velocity v_p in Eq. (17) as follows:

$$p^{(i+1,j)} = p^{(i,j)} + v_p^{(i,j)} \quad i = \{1, 2, \ldots n_{cmax} - 1\}, j = \{1, 2, \ldots n_{pt}\} \tag{18}$$

Because the three controllers triggered in multilevel variable control model depend on accumulated kinematic variations, the control accuracy of impulse-discharge power can be assured when their output ratios reach optimal values simultaneously. Thus the corresponding intelligent tuning scheme by utilizing particle swarm algorithm is described in Fig. 5 as follows:

1) Initial parameters of minimum global fitness value $F_{gmin} = 0.05$, maximum iterations $n_{cmax} = 100$, population number for each output ratio $n_p = 2$ and available evolutionary velocity $v_p\in$ [−1,1] are set to initialize particle swarm algorithm. 2^5 groups of population particles X are generated randomly for the output ratios of controller A (K_v, K_{i1}), controller B (K_n, K_{i2}) and of controller C (K_{i3}).
2) For the jth population particle at the ith iteration $X^{(i,\,j)}$, the multilevel variable control model is employed to obtain simulative impulse-discharge power curves in the case of $P_0 = 61, 62, \ldots, 85$ W and calculate the individual fitness value f_{obj} by the objective function in Eq. (15), respectively. The total fitness value $F_{obj}^{(1,\,j)}$ in Eq. (16) is evaluated utilizing the twenty-five results of f_{obj}. This step is repeatedly executed until the cycle index j reaches the total particle number n_{pt} of controller.
3) At the 1st iteration, the current position $p^{(1,\,j)}$ and $F_{obj}^{(1,\,j)}$ of particle $X^{(1,\,j)}$ are labeled as partial best position $p_{best}^{(j)}$ and fitness value $F_{best}^{(j)}$, respectively. Global best position p_{gbest} and fitness value F_{gbest} of all the particles are found by comparing to the $F_{best}^{(j)}$. At the 2nd iteration and more, the $p_{best}^{(j)}$ and $F_{best}^{(j)}$ are updated from the particle $X^{(i,\,j)}$ when the current $F_{obj}^{(i,\,j)}$ of particle $X^{(i,\,j)}$ is less than the labeled $F_{best}^{(j)}$. Further, the p_{gbest} and F_{gbest} are updated when the new $F_{best}^{(j)}$ is less than the labeled F_{gbest}.
4) The jth population particle at the i + 1th iteration $X^{(i+1,\,j)}$ is calculated by utilizing the evolutionary velocity $v_p^{(i,\,j)}$ in Eq. (17). The algorithm is repeatedly executed from step 2) to step 3) until the cycle index i reaches the n_{cmax} or the labeled F_{gbest} is less than the F_{gmin}. Finally, the labeled p_{gbest} of all the particles is output to determine the best output ratios of controller.

4. Development of impulse-discharge thermochemical truing system

Based on the above-mentioned multilevel variable control model, an impulse-discharge thermochemical truing system was developed by designing the specific monitoring and acquisition software to communicate SMART B818 grinder, DCS150-20E power supply and DS2102E

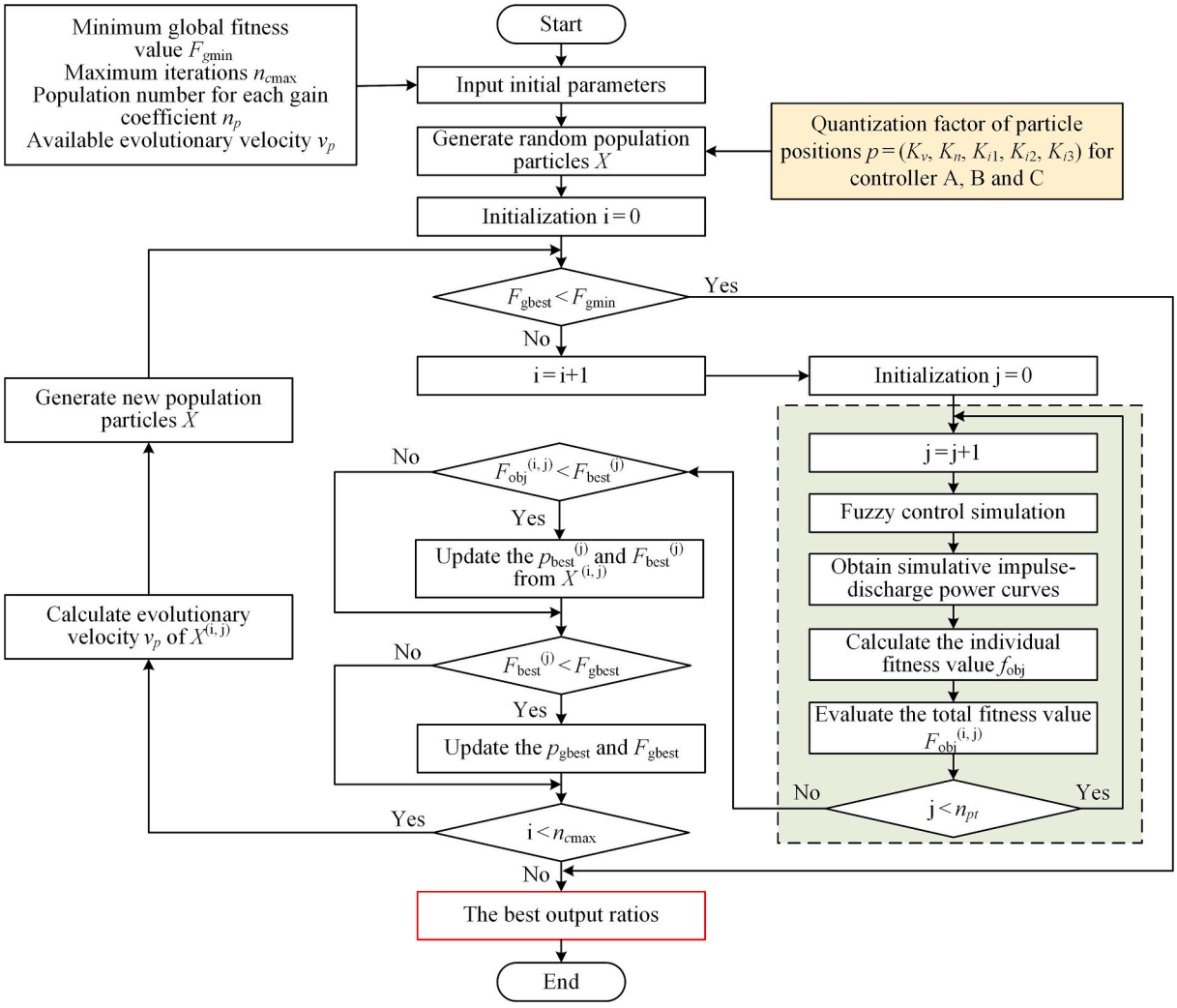

Fig. 5. Intelligent tuning scheme of output ratios of feed rate variation K_v, wheel speed variation K_n and limited current variation $K_{i1,\ 2,\ 3}$ by particle swarm algorithm.

oscilloscope with computer (see Fig. 6). It consists of four functional modules including impulse-discharge trace module, truing process analysis module, kinematic variable adjustment module and electrical variable adjustment module.

The impulse-discharge trace module is utilized to collect the impulse-discharge signal of RP1025D voltage sensor (range: ±50 V) and RP1001C current sensor (range: 10 mV/A) with sampling rate of 500 kHz and store it to the truing process analysis module with minimum time interval of 1 s. Based on the impulse-discharge signal processing, the multilevel variable control method with fuzzy logic is performed by truing process analysis module to output new truing variables. They are transmitted to the kinematic variable adjustment module and the electrical variable adjustment module for impulse-discharge power control. Herein, the minimum resolutions of feed rate v_f, wheel speed N and open circuit voltage E_i, limited current I_i are set as ±10 mm/min, ±100 rpm, ±0.1 V and ± 0.001 A, respectively, depending on the system performance.

To trace the impulse-discharge thermochemical truing process, the time-varying curves of impulse-discharge power P, feed rate v_f, wheel speed N and limited current I_i are displayed in a multiparameter visual interface of truing process analysis module. Besides, the grain top height h_g and area s_g regarded as mean values of the whole trued diamond grains on wheel surface could be recognized by He et al. [27] through the impulse-discharge signal. The h_g is calculated by Eqs. (3a), (3b), while the s_g is described based on the grain cutting temperature rate T in Eq. (1) as follows:

$$s_g^{(k)} = \begin{cases} s_{gd}, & k = 0 \\ \left[\sqrt{\frac{3}{2} s_{gd}} + \frac{7.8 \times 10^{-7} \left(\sqrt{s_{gt}} - \sqrt{s_{gd}} \right)}{h_r} \sum_{i=1}^{k} \left(T^{(i-1)} s_g^{(i-1)} - T_{cr} s_g^{(i-1)} \right) \right]^{\frac{2}{3}}, & k = \{1, 2, \cdots, n_w\} \end{cases} \tag{19}$$

where n_w is wheel revolution number. The total grain truing height h_r = 40 μm, grain top areas $s_{gd} = 3.5 \times 10^3$ μm^2 and $s_{gt} = 36 \times 10^3$ μm^2 before and after truing were taken as constants for 350-μm-size diamond wheel.

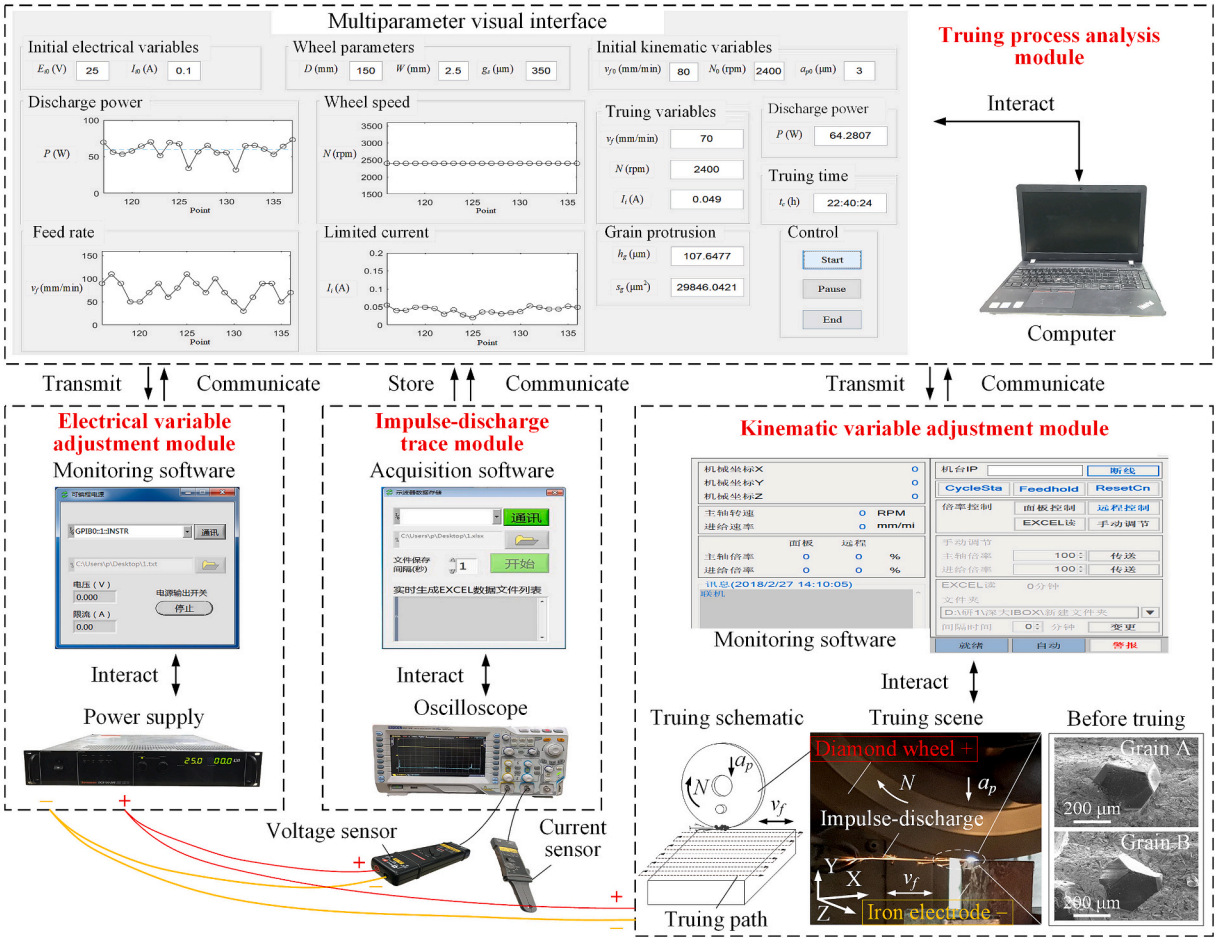

Fig. 6. Components of impulse-discharge thermochemical truing system.

5. Simulations and experiments

The multilevel variable control simulations and experiments with fuzzy logic for impulse-discharge thermochemical truing includes three parts. Firstly, the influence of feed rate v_f, wheel speed N and limited current I_i on discharge voltage U_c was investigated to give the discharge voltage sensitivity u (Part A). Secondly, the multilevel variable control process was simulated and the dynamic response of simulative impulse-discharge power P was analyzed to determine the output ratios of controllers through intelligent algorithm of particle swarm optimization (Part B). Thirdly, the impulse-discharge power P was traced by truing time t_c to validate the multilevel variable control effect (Part C).

In the experiments of Part A, the impulse-discharge thermochemical truing system was employed to true the 350-μm-size diamond wheel (#46, metallic bond, $W = 2.5$ mm, $D = 150$ mm, +, red line) in air with iron electrode (45# carbon steel, −, orange line), and the X-axial feed with Z-axial interval $\Delta z = 1$ mm was designed as truing path. The experimental conditions of No. 1–3 were listed in Table 1. To show the arc-discharge and spark-discharge voltages U_c in the same graph with small amount of experimental data, the kinematic variables K and the electrical variables E should be carefully chosen based on the grain top height h_g. Before truing, the diamond wheel was dressed for 3 h by 150–181-μm-size green silicon carbide oilstone (#80–100) to make the circular run-out <60 μm, its surface topography with initial grain top height $h_{g0} \approx 115$ μm and area $s_{g0} \approx 9.2 \times 10^3$ μm was showed in Fig. 6.

In the simulations of Part B, a Matlab software was utilized to design the multilevel variable control model in Fig. 3. The simulation time t_s was taken as 4 s for output ratio truing and 10 s for the control effect validation of impulse-discharge power. Herein, the four groups of random output ratios of $K_v = 1.5$, 3, 2 and 0.5, $K_n = 1.5$, 3, 2 and 1.5, and $K_{i1,\ 2,\ 3} = 3$, 2, 0.8 and 0.8 were set to obtain simulative impulse-discharge power P at disturbed discharge power $P_0 = 70$ W ($t_s = 0$–4 s), 60 W ($t_s = 4$–7 s) and 75 W ($t_s = 7$–10 s) against the trued ones.

In the experiments of Part C, two 350-μm-size diamond wheels were trued by utilizing and not utilizing multilevel variable control method, respectively. The corresponding experimental conditions of No. 4–5 were listed in Table 1. To illustrate the necessity of impulse-discharge power control, the diamond protrusion topographies were also observed by FEI Quanta 200 scanning electron microscope (SEM, mag: ×200) to measure the grain top area s_g. Herein, the two-dimension edge vertex coordinates (x_i, y_i) of diamond grain top were extracted in the image to calculate the s_g by utilizing Eq. (20). While the corresponding error rate mainly depended on the extraction accuracy of edge vertex, which was negligible because the diamond grain top with a clear plane profile could be easily recognized after truing. Considering the influence of irregularly distributed diamond grains, the permissible impulse-discharge power relative errors from 1 % to 7 % were investigated to

Table 1
Experimental conditions of part A and part C.

No.	N (rpm)	v_f (mm/min)	a_p (μm)	E_i (V)	I_i(A)	t_c (min)
1	900–3600	60	3	25	0.1	–
2	2400	30–120	3	25	0.1	–
3	2400	80	3	25	0.03–0.12	–
4	2400	80	3	25	0.1	2400
5	Time-varying	Time-varying	3	25	Time-varying	2400

assure the feasibility of controller before the experiments. Besides, the dry plunge grinding of hardened steel (53 HRC) at $N = 2400$ rpm, $v_f = 500$ mm/min, $a_p = 5$ μm and $\Delta z = 100$ μm was performed by utilizing the trued diamond wheels and theirs surface roughness Ra was measured by SJ210 profilometer (sample length: 0.25 mm), followed with the stability analysis of grinding process.

$$s_g^* = \frac{1}{2}\sum_{i=1}^{a-1}(x_i y_{i+1} - x_{i+1} y_i) \tag{20}$$

where s_g^* is measured grain top area, a is edge number of grain top profile, x_i and y_i are X-axial and Y-axial coordinate values of edge vertex, respectively.

Based on the previous research, each impulse-discharge happens at extremely short duration of 50–200 μs under the dynamic grain-electrode interaction, but it is difficult to trace the whole impulse-discharges timely. Fortunately, the unchanged grain protrusion could be assumed at a short truing time due to the nanoscale diamond thermochemical removal and wheel bond removal per wheel revolution. Thus the impulse-discharge signal was collected intermittently with 30-s interval rather than continuously trace in the long-time truing, and the trigger judgment of multilevel variable control was conducted with 10-min interval after analyzing the twenty on-site signals.

To trace the thermochemical removal of 350-μm-size diamond cutting edges, the critical grain cutting temperature rate $T_{cr} = 51.6$ °C per wheel revolution was determined by He et al. [27]. Generally, a selectable range of grain top area $s_g \in [20 \times 10^3, 50 \times 10^3]$ should be determined due to the limited spark-discharge voltage of 19–23 V and current of 2–4 A. Thus the target impulse-discharge power P_{tar} in Eq. (2) is described as follows:

$$P_{tar} = 0.002 s_g - 9.94 \quad s_g \in [20 \times 10^3,\ 50 \times 10^3] \tag{21}$$

In this study, the required grain top area $s_g = 35 \times 10^3$ μm^2 was determined to calculate the target impulse-discharge power $P_{tar} \approx 60$ W in multilevel variable control by Eq. (21). Further, the discharge voltage U_c of 20 ± 0.5 V was given at initial electrical variables E_0 of $E_{i0} = 25$ V and $I_{i0} = 0.1$ A. Thus the required kinematic variables (N, v_f, a_p) in Eq. (4) conforming to the initial grain top height h_{g0} are described as follows:

$$\left(0.0116h_{g0} - 0.558\right)^6 \le \frac{v_{f0}a_{p0}^2}{N_0}\frac{v_{f0}a_{p0}^2}{N_0} \le \left(0.0116h_{g0} - 0.479\right)^6 \tag{22}$$

At the initial grain top height $h_{g0} \approx 115$ μm, the initial kinematic variables K_0 of $N_0 = 2400$ rpm, $v_{f0} = 80$ mm/min and $a_{p0} = 3$ μm in the multilevel variable control were determined by Eq. (22). Herein, the a_{p0} of 3 μm could guarantee enough positive and negative variations of the other kinematic variables. For impulse-discharge thermochemical truing, the impulse-discharge power depends on kinematic and electrical variables in relation to grain top height, but the randomness of grain protrusion results in a bad mapping relationship. This means the same kinematic and electrical variables may product different impulse-discharge powers. Thus the intelligent algorithms such as neural network, etc. are not suitable to control the impulse-discharge power without large amount of sample data.

6. Result and discussion

6.1. Discharge voltage sensitivity for impulse-discharge power control

To obtain the discharge voltage sensitivity u in Eq. (6), the discharge voltage U_c was investigated at different truing variables. It is shown that the discharge voltage U_c decreased with increasing the feed rate v_f (see Fig. 7a), while increased with increasing the wheel speed N (see Fig. 7b) and limited current I_i (see Fig. 7c). A threshold of 18 ± 0.5 V was determined by He et al. [28] to transfer the spark-discharge into arc-discharge. In the case of spark-discharge, there existed clear linear correlations between discharge voltage and truing variables. This means that the complex system disturbance caused by grain protrusion uncertainty in the truing process may be compensated by adjusting the truing variables. Besides, the corresponding fitting curves could be given in Eqs. (23)–(25) by utilizing a least square method as follows:

$$U_c(v_f) = -0.05 v_f + 24.64 \tag{23}$$

$$U_c(N) = 0.0025N + 14.62 \tag{24}$$

$$U_c(I_i) = 42.35 I_i + 17.63 \tag{25}$$

Based on the fitting curves in Eqs. (23)–(25), the discharge voltage sensitivities u of feed rate v_f, wheel speed N and limited current I_i are taken as $u_{vf} = -0.05$ V/(mm·min^{-1}), $u_N = 0.0025$ V/rpm and $u_{Ii} = 42.35$ V/A, respectively. Herein, the feed rate v_f at minimum resolution presents the most significant effect for impulse-discharge power control. When the accumulated $\Delta v_f = \pm 70$ mm/min, $\Delta N = \pm 600$ rpm and $\Delta I_i = \pm 0.08$ A are set in multilevel variable control model, the corresponding impulse-discharge power variations ΔP could be given with $\Delta P_{vf} = \pm 10.5$ W, $\Delta P_N = \pm 4.5$ W and $\Delta P_{Ii} = \pm 10$ W. The aggregate value of ± 25 W conforms to the control requirement. For actual application, the available control range of impulse-discharge power error e_p also depends on the initial truing variables. When the three truing variables of v_f, N and I_i are beyond their adjustable ranges, the cutting depth a_p should be redetermined to update the adjustable ranges. This is the reason to integrate the diamond thermochemical removal mechanism and experimental data in multilevel variable control of impulse-discharge power with fuzzy logic.

It has been reported by He et al. [27] that the increased discharge voltage U_c might enhance the thermal energy to produce more diamond thermochemical removal for larger grain top area in reference to the diamond thermal transmission balance. Accordingly, the above-

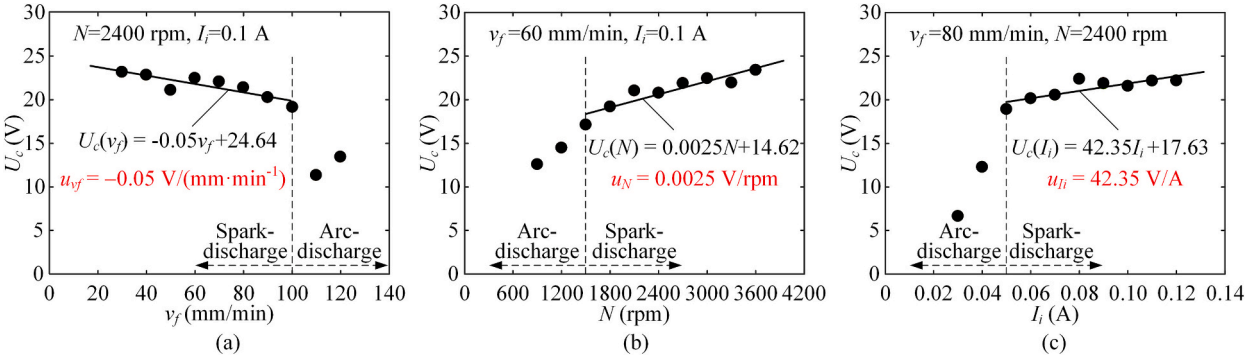

Fig. 7. Discharge voltage sensitivity u in relation to experimental results between discharge voltage U_c and truing variables. (a) Feed rate v_f. (b) Wheel speed N. (c) Limited current I_i.

mentioned correlations are utilized to design the fuzzy rules in Fig. 2. Even though the limited current adjustment presented the best system stability regardless of the discharge gap, it might aggravate wheel bond removal and finally lead to shedding grains [28]. This is because the small discharge gap is apt to enhance the impulse-discharge thermal transmission to wheel bond. Accordingly, the controller A with feed rate v_f, the controller B with wheel speed N and the controller C with limited current I_i are advised in sequence. To assure the system control efficiency, the limit current I_i is slightly adjusted in controller A. Considering the impulse-discharge power error e_p for each control less than ±10 W, the feed rate variation Δv_f is determined as NS or PS, and the limited current variation ΔI_i is ZO to avoid the overshoot at the small e_p = NS or PS. It has also been known that the kinematic variable adjustment may not acquire expected cutting chip height to accurately compensate the grain protrusion uncertainty because of the limited kinematic resolution of grinder. While the impulse-discharge power could be regulated by adjusting limited current I_i regardless of the discharge gap. This is the other reason to add the limited current adjustment in controller A. Further, the Δv_f is NB or PB and the ΔI_i is PS or NS at the middle e_p = NM or PM. Except the uncertain discharge gap in impulse-discharge thermochemical truing, the constant-voltage/constant-current transform of DC power supply also makes the impulse-discharge power fluctuate seriously due to the suppressed arc-discharge. It may be eliminated by adjusting the feed rate slightly (see Fig. 7a). To take the two factors into consideration, the Δv_f is NS or PS and the ΔI_i is PB or NB at the big e_p = NB or PB. This strategy is suitable to design the fuzzy rules of controller B. For controller C, the ΔI_i is PS or NS at the small e_p = NS or PS and the middle e_p = NM or PM, while the ΔI_i is PB or NB at the big e_p = NB or PB.

6.2. Tuned output ratios related to truing variable adjustment

The multilevel variable control model with fuzzy logic was utilized to intelligently tune the five output ratios (K_v, K_n, K_{i1}, K_{i2}, K_{i3}) through particle swarm algorithm. Before simulation, it is necessary to determine the transfer function of impulse-discharge power G_p (s) in Eq. (14). Accordingly, the rise time t_r = 2.8 ms and peak time t_p = 2.85 ms were given by analyzing the dynamic characteristics of impulse-discharge in the case of N = 2400 rpm, v_f = 100 mm/min, a_p = 1 μm, E_i = 40 V and I_i = 0.1 A (see Fig. 4). Hence, the transfer functions related to feed rate v_f, wheel speed N and limited current I_i could be given in Eqs. (26)–(28) as follows:

$$G_{p\text{-}vf}(s) = \frac{-0.15}{0.0036s^2 + 0.12s + 1} \tag{26}$$

$$G_{p\text{-}N}(s) = \frac{0.0075}{0.0036s^2 + 0.12s + 1} \tag{27}$$

$$G_{p\text{-}Ii}(s) = \frac{127.05}{0.0036s^2 + 0.12s + 1} \tag{28}$$

According to the transfer functions in Eqs. (26)–(28), the response curves of impulse-discharge power variation ΔP are given in the ranges of feed rate variation $\Delta v_f \in [-80, 80]$, wheel speed variation $\Delta N \in [-600, 600]$ and limited current variation $\Delta I_i \in [-0.08, 0.08]$, respectively. The ΔP trends to be a stable value at the simulation time of 0.5 s. This means the trigger delay t_d for each discharge power control should be set as t_d = 0.5 s in the multilevel variable control model.

Through the particle swarm algorithm in Fig. 5, the five tuned output ratios were determined as K_v = 0.9, K_n = 2.2, K_{i1} = 3.9, K_{i2} = 3.5 and K_{i3} = 0.6. Accordingly, the mapping relationships between impulse-discharge power error e_p and feed rate variation Δv_f, wheel speed variation ΔN and limited current variation ΔI_i could be drawn by utilizing the fuzzy rules of three controllers (see Fig. 8). It is shown that the limit values of feed rate variation Δv_f = −40 mm/min and 40 mm/min are achieved at impulse-discharge power errors $e_p \in [-6.7, -6.6]$ and [6.6, 6.7], while the limit values of wheel speed variation ΔN = 900 rpm and − 900 are achieved at $e_p \in [-6.8, -6.6]$ and [6.6, 6.8].

Further, the limited current variations ΔI_i of controller A and B maintain at zero until the e_p is beyond ±3.4 W and ± 3.5 W, respectively. It conforms to the requirement of impulse-discharge power control in the thermochemical truing. Moreover, the Δv_f of controller A, the ΔN of controller B and the ΔI_i of controller C begin to change when the e_p reaches ± 0.7 W, ± 0.2 W and ± 1.3 W, respectively, due to their minimum revolutions. This means the three controllers are not triggered at a small impulse-discharge power error.

6.3. Dynamic response of impulse-discharge power with truing variable adjustment

Fig. 9 shows the simulative impulse-discharge power P of multilevel variable control model with 60 W target value by utilizing the tuned output ratios in contrast to the random ones. It is shown that the simulative P of the first group of random output ratios fluctuates between 59.4 W and 60.8 W when it decreases from 70.0 W at the disturbed impulse-discharge power P_0 = 70 W. The fluctuation is attributed to the feed rate variation Δv_f = ± 10 mm/min (see Fig. 9b). Moreover, the simulative P increases from 49.4 W to 61.6 W and finally maintains at 60.1 W after three trigger times at the P_0 = 60 W. The overshoot of 1.6 W is produced at the 2nd trigger time due to large Δv_f of −40 mm/min (see Fig. 9b). At the P_0 = 75 W, the simulative P decreases from 75.1 W to 60.3 W with 0.5 % steady-state error after three trigger times. Herein, the wheel speed variation ΔN of −200 rpm is output at the 3th trigger time because the accumulated Δv_f reaches 70 mm/min (see Fig. 9c). Although the second group of random output ratios can control the simulative P to target value with only one trigger time at the P_0 = 70

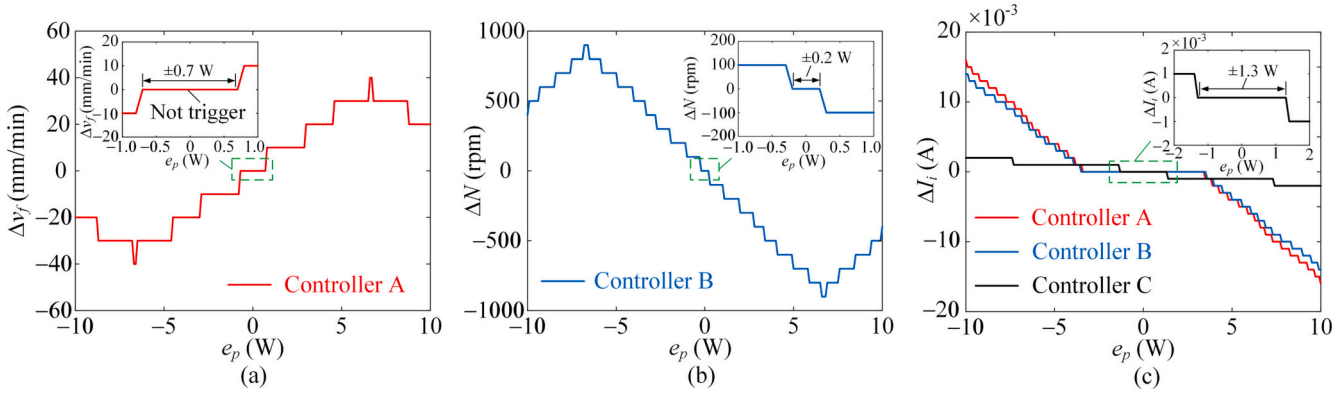

Fig. 8. Tuned mapping relationships between impulse-discharge power error e_p and truing variations. (a) Feed rate variation Δv_f. (b) Wheel speed variation ΔN. (c) Limited current variation ΔI_i.

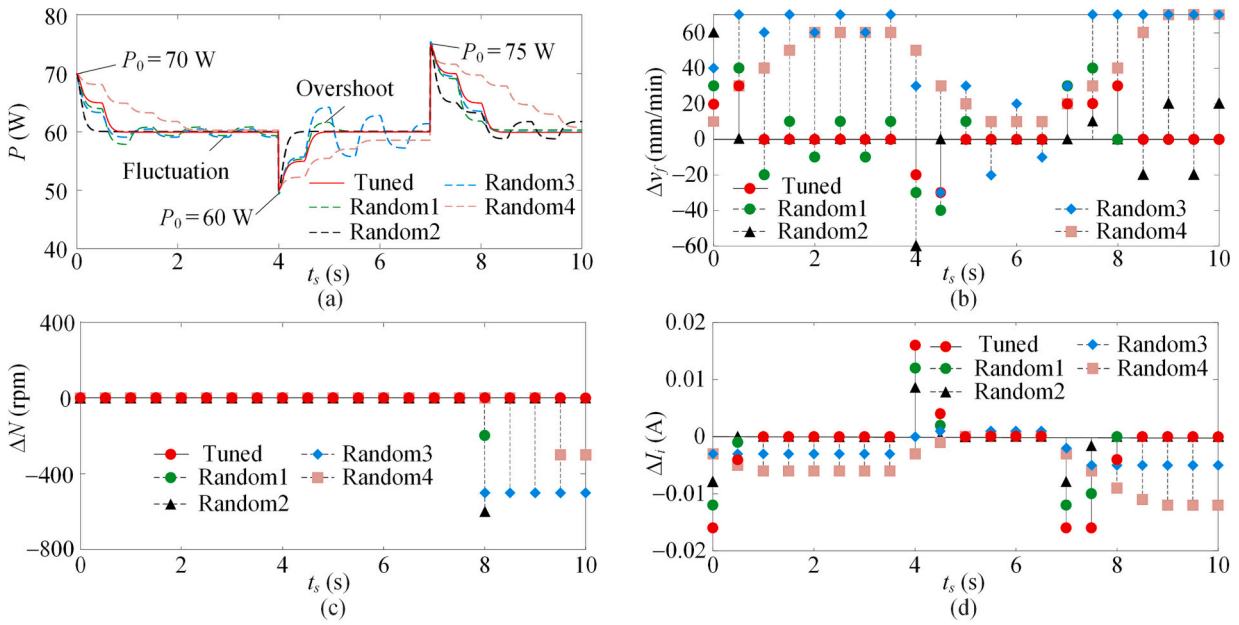

Fig. 9. Simulative results for multilevel variable control with tuned and random output ratios. (a) Simulative impulse-discharge power P. (b) Feed rate variation Δv_f. (c) Wheel speed variation ΔN. (d) Limited current variations ΔI_i.

W and 60 W, respectively, it is useless at the $P_0 = 75$ W. The other three groups of random output ratios also reveal the similar results in the simulation. Through the above-mentioned analysis, the random output ratios could not assure stable performance of controller at different disturbed impulse-discharge power.

In contrast to random output ratios, the tuned ones make the simulative P approach to target value of 60 W without any overshoot under the three disturbances. The corresponding steady-state errors are 0.07 %, 0.02 % and 0.12 % after two, two and three trigger times, respectively. Although the tuned output ratios present a minor disadvantage on larger range of $\Delta I_i \in [-0.016, 0.016]$ against the random ones of $\Delta I_i \in [-0.012, 0.012]$ (see Fig. 9d), the simulative P could be stabilized faster. This means the tuned output ratios may meet different disturbances with small steady-state errors, few trigger times and no overshoot for impulse-discharge power control.

6.4. Experimental validation on multilevel variable control of impulse-discharge power

To analyzing the feasibility of multilevel variable control method, the controller with different permissible errors was utilized to regulate the measured impulse-discharge discharge power P^* towards the target value P_{tar} of 60 W as shown in Fig. 10. It is shown that the controller was triggered 11 times and 10 times at the permissible errors of 1 % and 3 %, respectively, but the measured P^* always fluctuated seriously. As the permissible error was set to 5 % and more, the controller could make the measured P^* stable. There exists a system error of impulse-discharge power which cannot be eliminated in-process due to the random grain

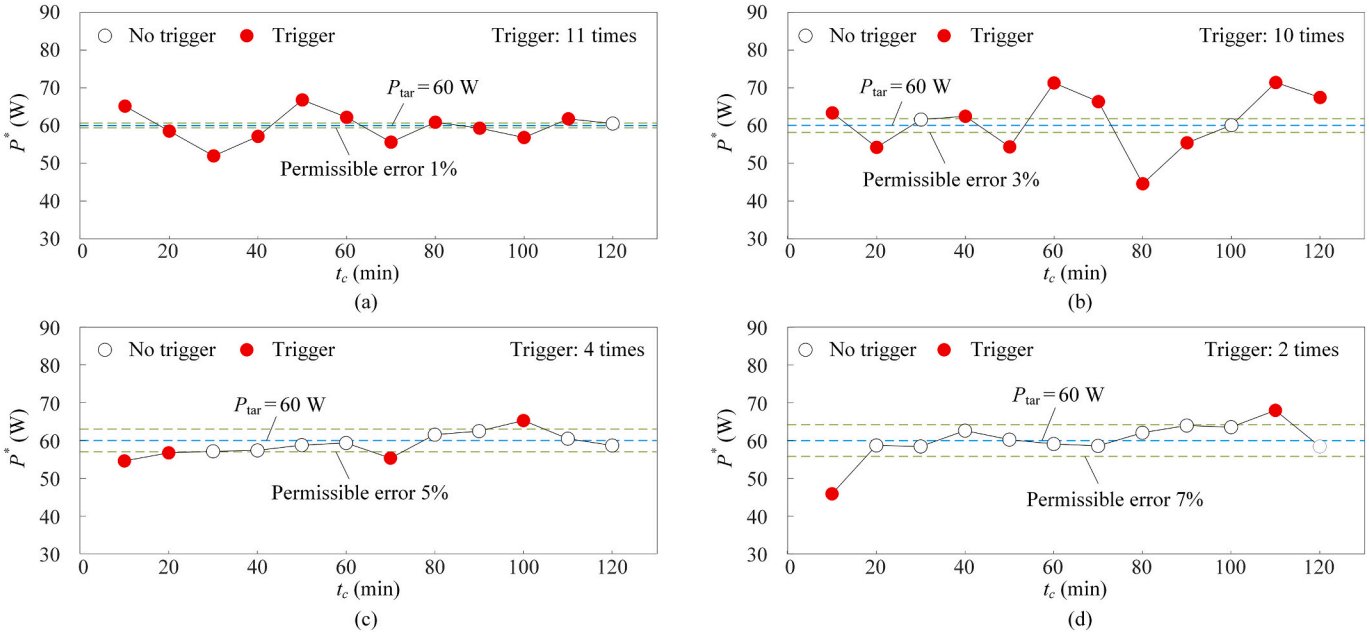

Fig. 10. Measured impulse-discharge power P^* for multilevel variable control with permissible error. (a) 1 %. (b) 3 %. (c) 5 %. (d) 7 %.

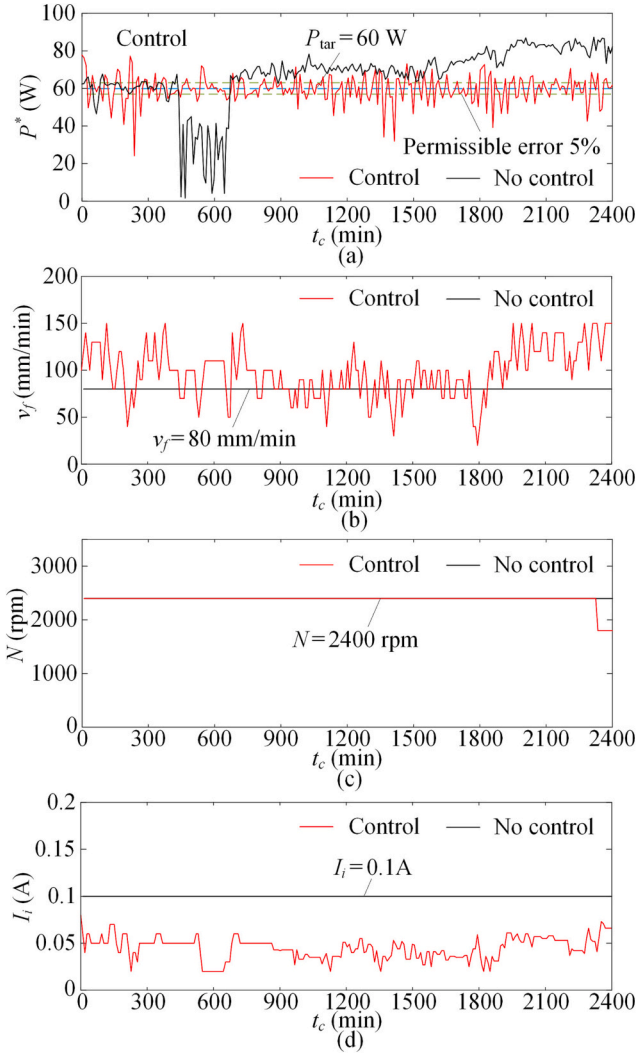

Fig. 11. Experimental results for multilevel variable control and no control. (a) Measured impulse-discharge power P^*. (b) Feed rate v_f. (c) Wheel speed N. (d) Limited current I_i.

distribution on wheel surface. This means the minimum accuracy of multilevel variable control depends on the system error in relation to grain size. This is the other reason why the PID method with high accuracy is not suitable to control impulse-discharge power. Thus the threshold of impulse-discharge power relative error in Fig. 2 was given by e = 5 % for controller triggering.

Fig. 11 shows the measured impulse-discharge power P^* of multilevel variable control with 60 W target value utilizing the tuned output ratios against the results with no control. The measured P^* with no control tended to be stable within 60 ± 3 W at the beginning of truing time t_c = 0–480 min, but it decreased seriously and even produced arc-discharge (<40 W) in the case of t_c = 480–720 min due to the uncertainties in truing process. In the case of t_c = 720–1920 min and 1920–2400 min, the measured P^* were fluctuating and approached to 69.5 W and 81.7 W in average, however, about 16 % and 36 % larger than the target value.

Under the multilevel variable control, the measured P^* could be regulated to target value with 5 % error by adjusting the feed rate v_f, wheel speed N and limited current I_i. While the N might not be adjusted at the impulse-discharge power error e >20 W, beyond the aggregate impulse-discharge power variations of $\Delta v_f = \pm 10.5$ W and $\Delta I_i = \pm 10$ W in simulation. This is because the chip accumulation sharply decreases the discharge gap to produce arc-discharge during truing, which can be suppressed by slightly changing the truing variables (see Fig. 7). For the impulse-discharge power error e not more than ± 5 W, the truing variables might be adjusted several times to make the measured P^* stable at 60 ± 3 W due to the influence of system error. Thus the multilevel variable control method confirms to the requirement for impulse-discharge power control.

Fig. 12 shows the diamond protrusion topographies with multilevel variable control in contrast to no control. It is shown that the irregular diamond cutting edges were on-machine truncated to be plane and reached to an isoheight line with good protrusion uniformity after truing. The mechanical action on graphitization layer removal contributed to the smooth diamond surface without damage [28]. Under multilevel variable control, the measured grain top area s_g^* reached 32.8 × 10^3 μm^2 in average, <7 % error of the required value of 35 × 10^3 μm^2. However, the measured s_g^* of 42.3 × 10^3 μm^2 with no control was quite larger than the target value caused by the uncontrollable impulse-discharge power in Fig. 11a. Further, the shedding grains were observed in Fig. 12a during truing with no control because large spark-discharge power might aggravate the wheel bond removal. Hence, it is necessary to control impulse-discharge power in thermochemical truing process, and the multilevel variable control method may assure the truing effect for required diamond cutting edges to achieve precision

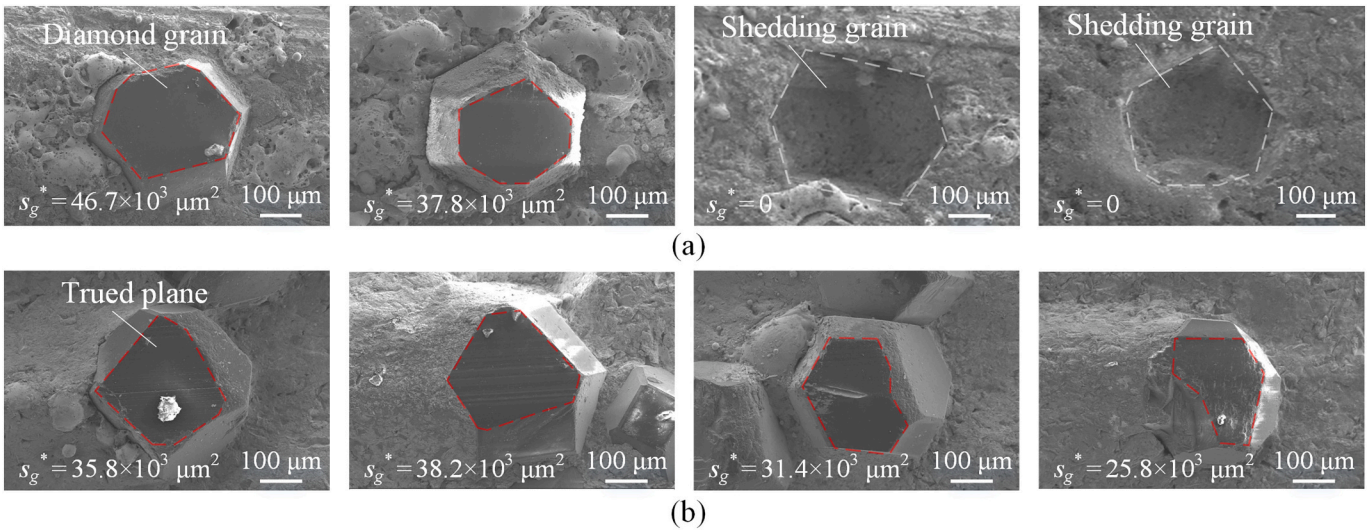

Fig. 12. Diamond protrusion topography. (a) No control. (b) Multilevel variable control.

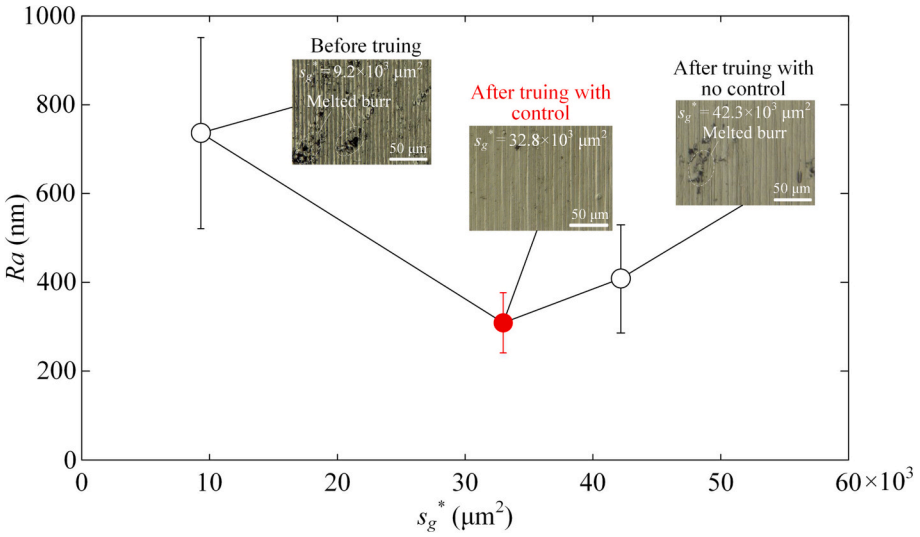

Fig. 13. Surface roughness *Ra* versus measured grain top area s_g^* in dry grinding of hardened steel.

grinding of difficult-to-cut metals.

Further, the diamond wheels after truing with multilevel variable control and no control were utilized to grind the hardened steel in dry medium against the one before truing, respectively. The corresponding surface quality is shown in Fig. 13. It is shown that the diamond grains after truing with multilevel variable control produced the smoothest surface without melted burr. The ground surface roughness of $Ra = 285$ nm was obtained, 62 % and 33 % lower than the 736 nm before truing and 424 nm after truing with no control, respectively. This is because the trued diamond grains in Fig. 12b may achieve the cutting-to-burnishing with thermal-force dispersion [32]. Herein, the increased grain top area not only diminishes the mechanical compression to trigger workpiece force dispersion, but also improves the thermal expulsion conditions to trigger workpiece thermal dispersion and diamond graphitization suppression. Besides, the diamond grains after truing with multilevel variable control made the grinding process stable with the smallest error bar of ± 66 nm in contrast to the ones of ± 224 nm before truing and ± 143 nm after truing with no control due to the more active grains on wheel surface and their high protrusion uniformity. It has been reported that the trued diamond grinding in dry medium decreased the surface roughness of hardened steel by about 1 time against the general CBN grinding in wet medium [28]. As a result, the multilevel fuzzy control of impulse-discharge power may guarantee the diamond cutting edges for stable dry smooth grinding so as to replace the general wet CBN grinding.

7. Conclusions

1) The kinematic and electrical variables are linearly related to the spark-discharge voltage that is characterized from the on-site impulse-discharge signal. The discharge voltage increases with increasing the wheel speed and limited current, while decreases with increasing the feed rate. Wherein the feed rate presents the most significant effect. The correlations may be utilized to control the impulse-discharge power during thermochemical truing.
2) The multilevel variable control process is modeled to tune the output ratios by the particle swarm algorithm. Compared to the random output ratios, the tuned ones improve the system control performance on impulse-discharge power at different disturbances caused by grain protrusion uncertainty. It significantly decreases the maximum steady-state error to 0.12 % with few trigger times and no overshoot.
3) In the thermochemical truing of 350-μm-size diamond wheel, the developed system with fuzzy logic is validated by stabilizing the impulse-discharge power towards target value of 60 W with 5 % permissible error. The knowledge-based control of impulse-discharge power may guarantee the required grain top area within 7 % error. It achieves the stable dry diamond grinding of hardened steel with surface roughness of 285 ± 66 nm to replace the general wet CBN grinding.

It has been known that the output ratios of designed fuzzy controller are determined based on the simulation model that is developed by the transfer functions of impulse-discharge power. While the discharge voltage sensitivities in the transfer functions are likely to be changed at different grain top heights. This means the designed fuzzy controller may be merely suitable for the diamond wheel with a certain range of grain top height. Hence, the self-adaptation control method with fuzzy logic will be further studied in the future by associating with the grain protrusion status. It may improve the process stability of impulse-discharge power for high-accuracy trace of grain top area.

Declaration of competing interest

The authors declare that they have no known competing financial interests or personal relationships that could have appeared to influence the work reported in this paper.

Acknowledgements

This work is supported by the National Natural Science Foundation of China (No. 51975219, No. 52375493), the Natural Science Foundation of Guangdong Province (No. 2023A1515011461), the Basic and Applied Basic Research Foundation of GuangDong Province (No. 2022A1515220053), and the Science, Technology and Innovation Commission of Shenzhen Municipality (No. JCYJ202208181004 12027, No. JCYJ20210324120402007).

Appendix A

Table 2
Parameters.

Parameters	Definition
a_p	Cutting depth (μm)
D	Wheel diameter (mm)
E_i	Open circuit voltage (V)
F_m	Cutting force (N)
G_e	Discharge gap (μm)
g_s	Grain size (μm)
h_f	Cutting chip height (μm)
h_g	Grain top height (μm)
I_c	Discharge current (A)
I_i	Limited current (A)
N	Wheel speed (rpm)
N_c	Active grain number for unit wheel width
P	Impulse-discharge power (W)
Ra	Ground surface roughness (nm)
s_g	Grain top area (μm^2)
T	Grain cutting temperature rate (°C per wheel revolution)
t	Sampling time (s)
t_c	Truing time (min)
t_s	Simulation time (s)
U_c	Discharge voltage (V)
u	Discharge voltage sensitivity
v_f	Feed rate (mm/min)
W	Wheel width (mm)
w_g	Grain top width (μm)

References

[1] Pervez MR, Ahamed MH, Ahmed MA, Takrim SM, Dario P. Autonomous grinding algorithms with future prospect towards SMART manufacturing: a comparative survey. J Manuf Syst 2022;62:164–85. https://doi.org/10.1016/j.jmsy.2021.11.009.

[2] Kusiak A. Smart manufacturing. Int J Prod Res 2017;56:508–17. https://doi.org/10.1080/00207543.2017.1351644.

[3] Khosravani MR, Nasiri S, Reinicke T. Intelligent knowledge-based system to improve injection molding process. J Ind Inf Integr 2022;25:100275.

[4] Mahajan KR, Knoppers GE, Oosterling JAJ, van Luttervelt CA. Knowledge based design of EDM electrodes for mould cavities pre-machined by high-speed milling. J Mater Process Technol 2004;149:71–6. https://doi.org/10.1016/j.jmatprotec.2004.02.007.

[5] Zheng C, Xing JJ, Wang ZX, Qin XS, Eynard B, Li J, et al. Knowledge-based program generation approach for robotic manufacturing systems. Robot Comput Integr Manuf 2022;73:102242. https://doi.org/10.1016/j.rcim.2021.102242.

[6] Fathima K, Schinhaerl M, Geiss A, Rascher R, Sperber P. A knowledge based feedback control system for precision ELID grinding. Precis Eng 2010;34:124–32. https://doi.org/10.1016/j.precisioneng.2009.05.004.

[7] Caraguay SJ, Boaron A, Weingaertner WL, Bordin FM, Xavier FA. Wear assessment of microcrystalline and electrofused aluminum oxide grinding wheels by multi-sensor monitoring technique. J Manuf Process 2022;80:141–51. https://doi.org/10.1016/j.jmapro.2022.05.052.

[8] Müller U, Prinz S, Barth S, Bergs T. Analysis of the thermo-mechanical load and productivity during force-compliant grinding of pcBN. J Mater Process Technol 2022;305:117604. https://doi.org/10.1016/j.jmatprotec.2022.117604.

[9] Huang XK, Chai Z, Ren XK, Chen XQ. A modified infrared emissivity model accurately determining dynamic temperatures for belt grinding Inconel 718. J Manuf Process 2023;101:86–103. https://doi.org/10.1016/j.jmapro.2023.05.091.

[10] Tang J, Qiao JF, Wu ZW, Chai TY, Zhang J, Yu W. Vibration and acoustic frequency spectra for industrial process modeling using selective fusion multi-condition samples and multi-source features. Mech Syst Signal Process 2018;99:142–68. https://doi.org/10.1016/j.ymssp.2017.06.008.

[11] Lee CW. On-line model identification for the machining process based on multirate process data. J Manuf Syst 2020;56:622–30. https://doi.org/10.1016/j.jmsy.2020.04.006.

[12] Lee CH, Jwo JS, Hsieh HY, LinCS.. An intelligent system for grinding wheel condition monitoring based on machining sound and deep learning. IEEE Access 2020;8:58279–89. https://doi.org/10.1109/ACCESS.2020.2982800.

[13] Ren HR, Guo W, Jiang PY, Wan X. An integrated approach of active incremental fine-tuning, SegNet, and CRF for cutting tool wearing areas segmentation with small samples. Knowl-Based Syst 2021;218:106838. https://doi.org/10.1016/j.knosys.2021.106838.

[14] Dai SJ, Li SN, Ji WB, Sun ZL, ZhaoYF.. Force tracking control of grinding end effector based on backstepping plus PID. Ind Robot 2022;49:34–46. https://doi.org/10.1108/IR-10-2020-0229.

[15] Zadeh LA. Outline of a new approach to the analysis of complex systems and decision processes. IEEE Trans Syst Man Cybern 1973:28–44. https://doi.org/10.1109/TSMC.1973.5408575 (SMC-3).

[16] Zadeh LA. Fuzzy algorithms. Inf Control 1968;12:94–102. https://doi.org/10.1016/S0019-9958(68)90211-8.

[17] Han JL, Liu YL, Luo LS, Mao MS. Integrated production planning and scheduling under uncertainty: a fuzzy bi-level decision-making approach. Knowl-Based Syst 2020;201:106056. https://doi.org/10.1016/j.knosys.2020.106056.

[18] Qi XZ, Sun Y, Ma XH, Hu Y, Zhang JW, Tian W. Multilevel fuzzy control based on force information in robot-assisted decompressive laminectomy. Int Orthod 2018;1093:263–79. https://doi.org/10.1007/978-981-13-1396-7_20.

[19] Li DH, Cao HR, Chen XF. Fuzzy control of milling chatter with piezoelectric actuators embedded to the tool holder. Mech Syst Signal Process 2021;148:107190. https://doi.org/10.1016/j.ymssp.2020.107190.

[20] Lin CJ, Lin CH, Wang SH. Using fuzzy control for feed rate scheduling of computer numerical control machine tools. Appl Sci Basel 2021;11:4701. https://doi.org/10.3390/app11104701.

[21] Wang XJ, Song QH, Gupta MK, Liu ZQ. Active vibration control of thin-walled milling based on ANFIS parameter optimization. Int J Adv Manuf Technol 2021;114:563–77. https://doi.org/10.1007/s00170-021-06900-2.

[22] Liang HB, Zou JL, Zuo K, Khan MJ. An improved genetic algorithm optimization fuzzy controller applied to the wellhead back pressure control system. Mech Syst Signal Process 2020;142:106708. https://doi.org/10.1016/j.ymssp.2020.106708.

[23] Kennedy J, Eberhart R. Particle swarm optimization. In: Proceedings of ICNN'95-international conference on neural networks. 4; 1995. p. 1942–8.

[24] Wang ZX, Mao JK, He ZZ, Liang FL. Fuzzy control based on IQPSO in proton-exchange membrane fuel-cell temperature system. J Energy Eng 2020;146:04020044. https://doi.org/10.1061/(ASCE)EY.1943-7897.0000691.

[25] Yang N, Huang W, Lei DJ. Control of nanoscale material removal in diamond polishing by using iron at low temperature. J Mater Process Technol 2020;278:116521. https://doi.org/10.1016/j.jmatprotec.2019.116521.

[26] Qian N, Fu YC, Jiang F, Ding WF, Zhang JZ, Xu JH. CBN grain wear during eco-benign grinding of nickel-based superalloy with oscillating heat pipe abrasive wheel. Ceram Int 2022;48:9692–701. https://doi.org/10.1016/j.ceramint.2021.12.170.

[27] He QP, Xie J, Huang JJ, Yang H, Xu XY. In-process monitoring of microscale grain protrusions by tracing impulse-discharge energy related to thermal transmission balance on diamond cutting interface. J Mater Process Technol 2021;297:117256. https://doi.org/10.1016/j.jmatprotec.2021.117256.

[28] He QP, Xie J, Lu K, Yang H. Study on in-air electro-contact discharge (ECD) truncating of coarse diamond grinding wheel for the dry smooth grinding of hardened steel. J Mater Process Technol 2020;276:116402. https://doi.org/10.1016/j.jmatprotec.2019.116402.

[29] Brinksmeier E, Riemer O, Rickens K, Berger D. Application potential of coarse-grained diamond grinding wheels for precision grinding of optical materials. Prod Eng Res Dev 2016;10:563–73. https://doi.org/10.1007/s11740-016-0699-y.

[30] Wu MT, Guo B, Zhao QL, Zhang J, Fang XY, He P. High efficiency precision grinding of micro-structured SiC surface using laser micro-structured coarse-grain

diamond grinding wheel. Int J Precis Eng Manuf Green Technol 2019;6:577–86. https://doi.org/10.1007/s40684-019-00058-9.
[31] Juang CF, Liou YC. On the hybrid of genetic algorithm and particle swarm optimization for evolving recurrent neural network. IEEE Int Joint Conf Neural Netw 2004:2285–9. https://doi.org/10.1109/IJCNN.2004.1380980.
[32] Yang H, Xie J, He QP, Liu JH, Shi YQ. Study on diamond cutting-to-burnishing for thermal-force dispersion in dry metal grinding. J Mater Process Technol 2023;313:117874. https://doi.org/10.1016/j.jmatprotec.2023.117874.